TU Dortmund

Case Studies

# Project 2: BTA Deep Hole Drilling

Lecturers:
Dr. Uwe Ligges
M. Sc. Marie Beisemann
M. Sc. Leonie Schürmeyer

Author: Tadeo Hepperle

Group number: 5

Group members:
Lennard Heinrigs, Tadeo Hepperle,
Joshua Oehmen, Vanlal Peka

July 26, 2023

# Contents

# 1 Introduction

BTA deep hole drilling is a machining process that is used to drill deep holes. A deep hole is a hole with a relatively large depth to diameter ratio. BTA stands for Boring and Trepanning Association. BTA drilling techniques can be used to create holes with a diameter of 6mm to 1500mm (SOURCE: Tiefbohrverfahren page 6). The material which is processed is typically metal and a depth to diameter ratio of up to 400:1 can be achieved (SOURCE: https://unisig.com/information-and-resources/what-is-deep-hole-drilling/what-is-bta-drilling/). In contrast to other drilling techniques, ususally the workpiece rotates around the drilling head. During the drilling process oil is injected into the drilled hole with high pressure. On the one hand the oil cools down the work piece that is heated up by the boring friction. On the other hand it also sweeps away metal chipping that is removed from the work piece by the BTA boring head.

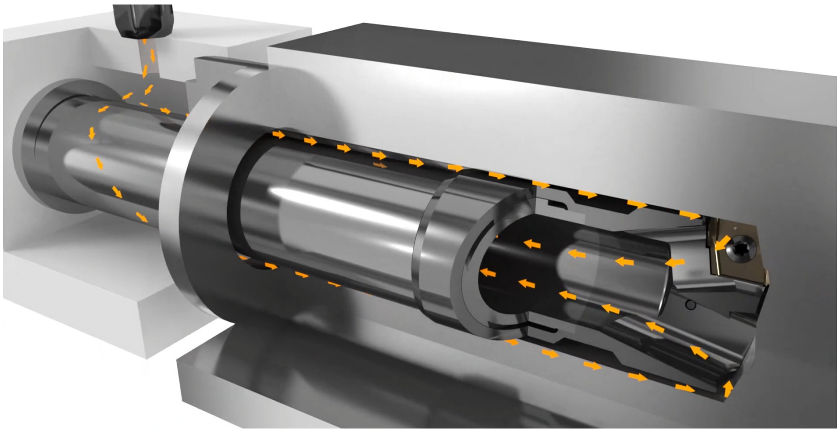

Figure 1: Oil flow in a BTA drilling head (**?**)

The yellow arrows in Figure **??** show the flow of oil in the process. Oil returns together with any removed metal chipping through the center of BTA tool. To support the BTA tool and reduce unwanted vibrations a damper may be used. In this report we take a look at BTA drilling processes with and without a damper. Because the holes in BTA drilling are so deep, the drilling head needs to be quite flexible: A drill that is too stiff could break from torsional forces easily. This flexibility comes at a disadvantage: the drilling head in a BTA machine needs to be self guiding and it is difficult to make sure that the hole is completely straight on such a long drilling path without any deviances at the hole borders.

The flexible drilling head can develop vibrations which lead to two undesired phenomenons: chatter and spiraling. Chatter can be described as "self-excited torsional

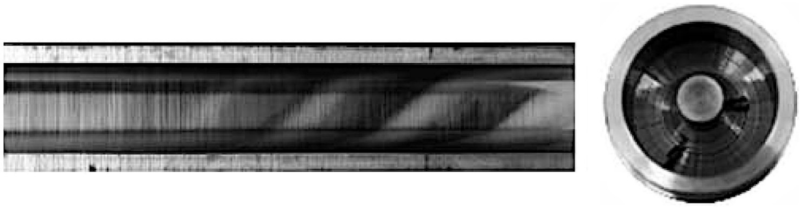

Figure 2: Spiraling (left) and Chatter (right) (?, p. 746)

vibrations" (SOURCE: DYNAMIC DISTURBANCES PAPER page 2). The torsional eigenfrequencies of the drilling tool lead to the edge of the drilling head chipping away material in an uneven way. The effect on the work piece can be seen in the right image in Figure ??. Chatter can be heard acousticly as a sort of humming. According to ?, p. 14, chatter is recognizable by the human ear as a "high-pitched tone which occurs during the process". Spiraling is caused by bending vibrations. The impairment ofthe bore hole can be seen on the left side of Figure ??. We do not have data on whether or not spiraling occured in the processes we analyze in this report and will thus not make statements about it. The main objective of this report is to find a good predictor of chatter and develop an early warning system to allow the BTA machine to be turned off before chatter causes too much damage to the work piece.

## 1.1 Prior Research

We now talk briefly about prior approaches that have been taken to detect chatter. ? propose to model chatter as a regenerative process. They run a chatter simulation that constantly updates the angle of the BTA tool, the cutting thickness and the drilling torque. They found that their physical model produces chatter similar to chatter in real world drilling processes regarding the drilling torque (?, p. 748). ? also experimented with predicting chatter in BTA processes. They found that the drilling torque is one of the most expressive signals for chatter detection. The other variables they looked at were force, acceleration in 3 directions and acoustic signals. Even though chatter can be recognized by pronounced frequencies on the acoustic channel, loud noise of other machinery in the factory makes it impractictical (?, p. 6). They found that the autocorrelation function for the drilling torque differs significantly between *chatter* and *non-chatter* segments of the BTA process. To predict chatter, an absolute sum of the ACF function ($A_{ACF}$-value) over 30 lags was used. When this value crossed a certain threshold a couple of times, it was a strong indicator of chatter appearing soon after.

To find the best decision rule based on the $A_{ACF}$ a neural network was used. **?**, p. 27 also found that the drilling torque is an important predictor of chatter and has shown that the spectrograms of the torque variable differ significanty between *chatter* and *non-chatter* time regions of the BTA process. Because of these findings we also expect the drilling torque (*moment* variable) to be of great use for chatter detection in this report.

## 1.2 The Data

To answer the question what causes chatter in BTA boring processes we take a look at data from 10 BTA drilling runs in this report. As shown in Table **??**, each process has its own identifier (e.g. *D4*), by which we refer to a process. We refer to the processes *D4*, *D6* and *D8* as *D*-processes, while *V2*, *V6*, *V10*, *V17*, *V20*, *V24* and *V25* are called *V*-processes. The *D*-processes were recorded in 2002 and featured a damper installed 1240 mm away from clamping. In contrast to that the *V*-processes were recorded in 2001 and did not use any damper in the BTA machine setup. It seems like the *D*-processes do not show signs of chatter, while we can observe some form of chatter in all *V*-processes.

Table 1: Drilling Processes and their Metadata

| *identifier* | *time* | *cutting speed* | *feed speed* | *oil pressure* |
|---:|---:|---:|---:|---:|
| *D4* | 3:54 min | 111 m/min | 0.231 mm/s | unknown |
| *D6* | 4:28 min | 120 m/min | 0.185 mm/s | unknown |
| *D8* | 4:27 min | 90 m/min | 0.250 mm/s | unknown |
| *V2* | 4:51 min | 120 m/min | 0.185 mm/s | unknown |
| *V6* | 4:25 min | 111 m/min | 0.231 mm/s | 371 l/min |
| *V10* | 4:25 min | 111 m/min | 0.231 mm/s | 229 l/min |
| *V17* | 4:44 min | 120 m/min | 0.185 mm/s | 300 l/min |
| *V20* | 4:58 min | 90 m/min | 0.250 mm/s | 300 l/min |
| *V24* | 4:29 min | 120 m/min | 0.185 mm/s | 300 l/min |
| *V25* | 4:33 min | 120 m/min | 0.185 mm/s | 300 l/min |

There are a few parameters that are chosen in advance for each drilling process: *cutting speed*, *feed speed* and *oil pressure*. Table **??** shows these parameters for the 10 processes. The data for each of the 10 processes consists of a time series recording of several variables. The time series data was recorded with a sampling rate of 20000Hz, so in each second of the boring process, 20000 observations of each of the measured variables have been recorded. That means there is no missing data and a consistent time gap of 0.05 ms between measurements. The time span of the drilling processes ranges from 3:54 min to

4:58 min. The data was recorded utilizing the *TEAC GX-1 Integrated Recorder* device, a machine developed by the *TEAC* electronics company. The distribution of the device has been discontinued (SOURCE: https://daqlogsystems.co.uk/product/teac-gx-1/). The machine features a set of up to 8 input channels that can be fed with analog data. Then, 16-bit A/D (analog to digital) converters convert the analog signal into a digital one, saving the measurement of each channel as a 16 bit signed integer. The associated coefficients to convert the physical value to an integer value and vice versa need to be specified before the recording starts. They can be used to restore continous physical values from the 16-bit measurements. The data is stored in an *interlaced* format. That means, for each point in time, the 16 bit value measured on each channel is appended to a file. So if we split the resulting file into chunks of $2 * NUMBER\_OF\_CHANNELS$ bytes, each of these chunks represents one point in time.

The following variables were measured for all 10 processes:

- *acoustic* - the audio signal in Pa (Pascal), noise and sound during the drilling process
- *moment* - the torsional moment in Nm (Newtonmeter), also known as drilling torque. Measured at the drilling bar above the bore hole of the BTA drilling machine. It is created by forces of chipping, friction and deformation at the guide rails.
- *sync signal* - an electric signal that is triggered by the drilling head having a certain axial rotation. It flows once per revolution of the drilling head for a brief moment.
- *oil acceleration* - the acceleration of the drilling oil supply in $m/s^2$
- *force* - the force in feed direction in N (Newton). It is related to the *feed speed* but also to the resistance (hardness) the work piece material has against being drilled

Besides that, the 7 $V$-processes feature 2 additional variables for the acceleration of the drilling head: *lateral acceleration* and *frontal acceleration* (acceleration in frontal direction) each measured in $m/s^2$. The 3 $D$-processes also contain the *bending moment* in Nm as a variable. They also contain measurements on a variable called "bohrst", but it remains unclear to us what this variable stands for. It is measured in $m/s^2$ but more we do not know, hence we do not further discuss it in this report.

### 1.2.1 Labels

The data we received is unlabeled. That means we just have the time series of the predictor variables, but do not know in what time regions chatter appears. The only thing we could do is listen to the audio signal. Because chatter can be heard as a resonating frequency, we were able to manually label each process and divide it into different time segments:

- *start* - before the boring head made contact to the material.
- *no chatter* - normal drilling, no audible chatter.
- *chatter* - audible chatter, recognizable as constistent high tones in the audio.
- *low chatter* - audible chatter, but rather low tones. Often present after some time of high tones chatter.
- *end* - after the boring head is done with drilling and no pressure is asserted on the material anymore

The time segments appear in each process in this order, sometimes skipping the *chatter* and *low chatter* stages. The main focus of this report is to detect the change from *no chatter* to *chatter* with some procedure that would work online only with data from **before** the *chatter* stage is entered.

# 2 Methods

This chapter briefly explains the statistical methods used. to apply them we use Python (**?**) as statistical software. The Python packages numpy (**?**), polars (**?**) and matplotlib (**?**) have been used. In addition to these, we developed a custom python package called *gx1convert* (**?**) that was used to read in the header and binary data produced by the GX-1 device (**?**).

## 2.1 Short-time Fourier Transform (STFT)

Short-time Fourier Transform (STFT) is a signal processing method that can be applied to a time series, to translate it from the time domain into a the frequency domain. Consider a discrete real valued discrete time series $X_t$. The STFT is defined as a function

$\mathbb{R} \to \mathbb{C}$, mapping each $X_t$ time point to a function $Y_t(\omega)$ that maps an angular frequency to a complex number. This complex number $z$ can be written in its Euler representation $re^{i\phi}$. We will discuss shortly how to interpret it. $Y_t(\omega)$ can be calculated with the following formula (?):

$$Y_t(\omega) = \sum_{t=-\infty}^{\infty} X_t w(n-m)e^{-j\omega t}$$

In this formula, $w(t)$ represents a window function that is shifted over all possible values of $t$ by an offset of $m$. A window function is a function that takes values between 0 and 1 in some range and returns 0 outside of that range. For the sake of simplicity, this can be thought of as a simple rectangular window, that returns 1 within a fixed range and 0 otherwise. In practice any window function can be used. Let $z = re^{i\phi}$ be the complex number that we get, when evaluating $Y_t(\omega)$ for some $\omega$ and a fixed point in time $t$. Then $r$ and $\phi$ represent the amplitude and phase of a sin wave with angular frequency $\omega$ at the time point $t$. The angular frequency $\omega$ can be converted to an actual frequency $f$ of our time series in Hz by $f = \omega\frac{s}{2\pi}$, where $s$ is the sampling frequency of the time series in Hz. Likewise if we want to know the STFT in a time point $t$ for any frequency $f$, we can use $\omega = f\frac{2\pi}{s}$ to calculate the corresponding radial frequency $\omega$ to pass to the $Y_t(\omega)$ function to obtain amplitude and phase.

The short-time Fourier transform can be used to represent the dominant frequencies of a time series over time with a spectrogram. A spectrogram can be plotted as a heatmap with the time $t$ on the x-axis, the frequency $f$ at the y-axis and the spectrogram value $S_{tf}$ represented by a color on a color spectrum. The spectrogram value $S_{tf}$ for a time point $t$ and a frequnecy $f$ is defined as the squared magnitude of the STFT $|Y_t(\omega)|^2 = |Y_t(f\frac{2\pi}{s})|^2$. It can be used to visualize how a frequency distribution in a time series behaves over time.

## 2.2 Covariance and Correlation

Given a set of $n$ datapoints each consisting of a value on two metric variables X and Y, their covariance $s_{XY}$ can be computed as the product of the difference to the respective variable mean summed up for all datapoints and divided by $n$.

$$s_{XY} = \frac{1}{n} \cdot \sum_{i=1}^{n} (x_i - \overline{x}) \cdot (y_i - \overline{y})$$

It is a measure of how much the variables vary together linearly in the same direction. Because the covariance greatly depends on the units of measurement, it can be standardized to a range between $-1$ and $+1$ by dividing it by the standard deviations of both variables.

$$r_{XY} = \frac{s_{XY}}{s_X \cdot s_Y}$$

The result $r_{XY}$ is known as Pearson's r or Pearson product-moment correlation coefficient. Note that $r_{XY}$ is symmetrical, so $r_{XY} = r_{YX}$ and in case that either $s_X$ or $s_Y$ is zero it is not defined. It is a standardized measure of linear correlation between two metric variables (**?**, p. 538). A correlation of $r_{XY} = 1$ means perfect correlation.

## 2.3 Auto-correlation Function (ACF)

The auto-correlation function (ACF) shows how much a time series is correlated with a lagged version of itself. For a Time series $X_t$ consisting of $n$ data points $x_1, ..., x_n$ the ACF is defined as a function $\rho(k)$ that maps an integer $k$ to the correlation of $X_t$ with $X_{t+1}$ (**?**, p. 4):

$$\rho(k) = Corr(X_t, X_{t+1})$$

In this equation, $k$ represents a lag value. In time series analysis we call a "lag", a shift of the time series along the temporal direction. The correlation is calculated over all possible values of $t$ where $1 \leq t \leq n - k$.For example for values $t = 3$ and $k = 2$, the variable $X_t$ would refer to the data point $x_3$ and $X_t$ would be $x_5$. From the equation follows that $\rho(0)$ is always 1, because $\rho(0) = Corr(X_t, X_t) = 1$. Because the ACF for higher lag values has less data point pairs available for correlation calculation, one should only calculate the ACF for lag values much less than the length of the time series itself. Interpreting the ACF only makes sense if the underlying process is (weakly) stationary (**?**, p. 4). This should be given if we look at regions of a drilling process where mean and variance do not change too much. Periodicities in a time series also show as periodic patterns in the ACF.

### 2.3.1 Absolute Area under the ACF ($A_{ACF}$)

**?** derived a value called $A_{ACF}$ from the auto-correlation function. They selected a range of L lags $k \in \{0, ..., L\}$ and calculated the ACF $\rho(k)$ for each lag value. Then they summed up the absolute value for each lag to obtain the $A_{ACF}$.

$$A_{ACF} = \sum_{h=0}^{L} |p(h)|$$

**?** chose a value of L=30 in their approach and calculated this $A_{ACF}$ value for small chunks of time cut out of the original time series. If there are strong resonating frequencies in the data (such as present during chatter), the $A_{ACF}$ value is expected to be high.

# 3 Data Analysis

We manually labeled each process as into segments as described in section **??**. Table **??** shows the time regions we determined for each segment in seconds:

Table 2: Time Segments of each Drilling Process

| | *start* | *no chatter* | *chatter* | *low chatter* | *end* |
|---|---|---|---|---|---|
| *D4* | 0 - 3 | 3 - 222 | / | / | 222 - 234 |
| *D6* | 0 - 2 | 2 - 254 | / | / | 254 - 268 |
| *D8* | 0 - 4 | 4 - 254 | / | / | 254 - 267 |
| *V2* | 0 - 10 | 10 - 200 | 200 - 264 | / | 264 - 291 |
| *V6* | 0 - 31 | 31 - 47 | 47 - 136 | 136 - 253 | 253 - 265 |
| *V10* | 0 - 31 | 31 - 47 | 47 - 91 | 91 - 252 | 252 - 264 |
| *V17* | 0 - 16 | 16 - 35 | 35 - 45 | 45 - 270 | 270 - 284 |
| *V20* | 0 - 33 | 33 - 52 | 52 - 136 | 136 - 287 | 287 - 298 |
| *V24* | 0 - 3 | 3 - 22 | 22 - 64 | 64 - 258 | 258 - 269 |
| *V25* | 0 - 5 | 5 - 118 | 118 - 260 | / | 260 - 272 |

The end point of the *start* segment and the start point of the *end* segment were best identified by looking at the *force* time series for each process. The force quickly increases in abolute value when the BTA drilling head makes contact with the workpiece and falls when it is released, as visible in Figure **??**. We also plotted the time series for *moment*, *sync signal*, *oil acceleration* and *acoustic* for all processes together with the time segements. They can be found in Figure **??** to Figure **??** in the Appendix. For the *V*-processes Figure **??** and Figure **??** show the frontal and lateral acceleration respectively. The reason for plotting all of these variables in conjuction with the time segments is, that it helps us identify which variables show a visible difference between the chatter and non-chatter regions. It looks like only the *acoustic* signal and the *moment* and *oil acceleration* show visible differences.

## 3.1 Frequencies and ACF

We now want to take a look at the frequency space. Figure **??** shows the spectrogram for the *V2*-Process. The area between the blue and purple line is the *non-chatter* segment, while the area between the purple and blue line marks the *chatter* segment. We can see that *force*, *moment*, *acoustic* and *oil acceleration* show changes in their pattern as soon as the chatter appears. But there does not seem to be a pattern forming, before the chatter starts.

If we assume that chatter is in general associated with the workpiece resonating certain frequencies, it is not surprising to see patterns to be more pronounced in the *chatter* segment. Using all data points from the *chatter* and *non-chatter* regions respectively we calculate the ACF up to lag 100 for each variable of the *V2*-process. We are looking for a variable where the ACF differs a lot between *chatter* and *non-chatter* regions. This would allow us then to witness how the ACF changes from its *non-chatter* form to the *chatter* constellation and shut down the machine before we fully reach the *chatter phase*.

Figure **??** and Figure **??** show a very regular periodic pattern in the ACF for the *chatter* phase for the variables *moment* and *oil acceleration*. The wavelength seems to be around 30 lags. Since $20000/30 \approx 667$ this lag constellation would suggest a dominant frequency of around 667 Hz. This is also visible as a thick black horizontal line in the *chatter* region of the top left spectrogram of Figure **??** (*moment* variable) at around this frequency. In the *non-chatter* regions the behavior of the ACF differs between the two variables though: *oil acceleration* shows some slowly decaying pattern, where after 100 lags almost no correlation is left, while we can observe some high frequent oscillations in the ACF of *moment*.

Figure **??** and Figure **??** shows that the ACFs of the *acoustic* and the *force* channel show similar behavior, but the ACF in the *chatter* region is not as regular as in the *moment* channel. The *sync signal*, *lateral acceleration* and *frontal acceleration* variables

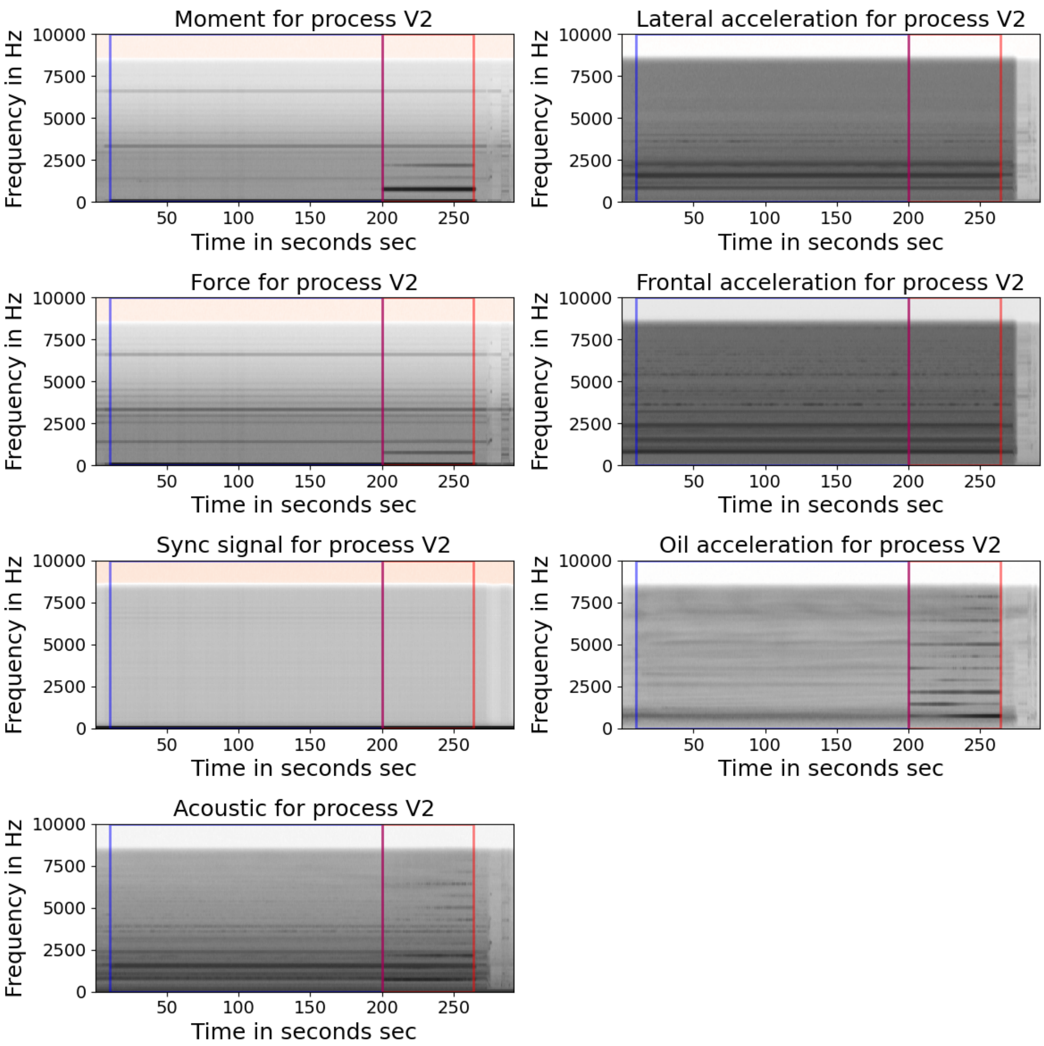


Figure 3: Spectrogram for the *V2*-Process

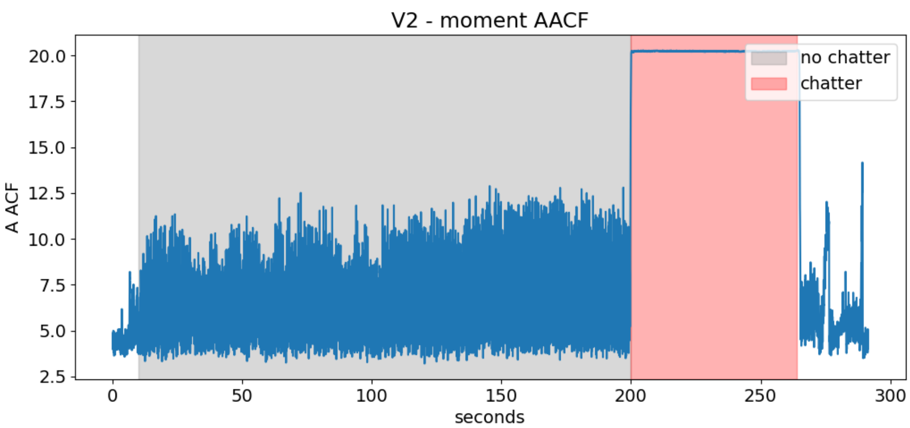


Figure 4: ACF for the *moment* variable of the *V2* process in two regions

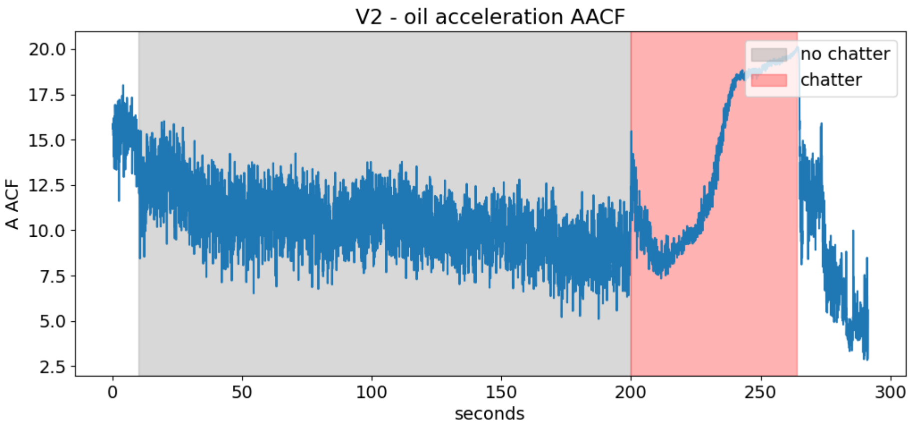


Figure 5: ACF for the *oil acceleration* variable of the *V2* process in two regions

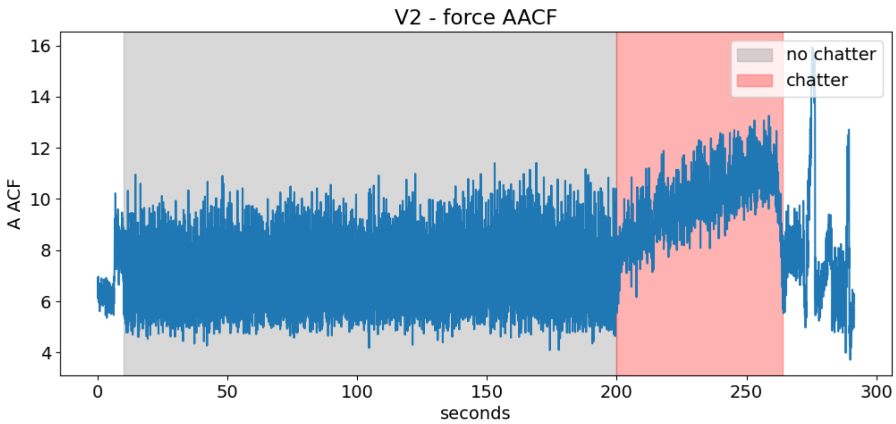


Figure 6: ACF for the *force* variable of the *V2* process in two regions

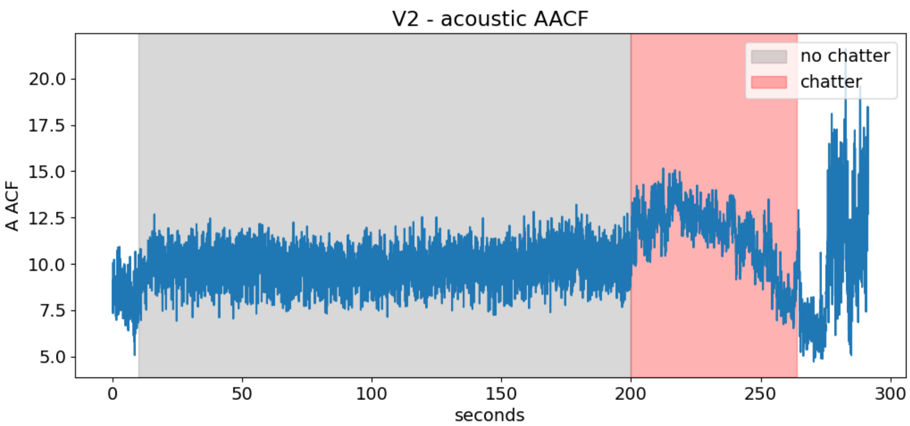


Figure 7: ACF for the *acoustic* variable of the *V2* process in two regions

are probably not very useful to detect chatter: The ACFs for *chatter* vs. *non chatter* segments in Figure ??, ?? and ?? do not really differ.

## 3.2 Detect chatter with $A_{ACF}$

We now split the time series into chunks with a width of 1000 data points. That is the equivalent of 50ms for each chunk. For each of these chunks we calculate the ACF up to lag 100. Using a similar approach as ? we reduce these 101 coefficients down to an $A_{ACF}$ value that represents the absolute area under the autocorrelation function $A_{ACF} = \sum_{h=0}^{L} |p(h)|$. Here $p(h)$ is the autocorrelation at lag $h$ calculated on the respective 1000-point chunk. Using this approach the *non-chatter* segments had between 320 and 3800 chunks and the *chatter* segments we composed of 200 to 2840 chunks each. Table ?? shows for each of the processes the average $A_{ACF}$ values in the *chatter* and *non-chatter* regions.

Table 3: $A_{ACF}$ from ACF up to lag 100 for *moment* in *non-chatter* and *chatter* segments. N = *non-chatter*, C = *chatter*

| process | *mean* | | *std* | | *min* | | *max* | |
|---|---|---|---|---|---|---|---|---|
| | N | C | N | C | N | C | N | C |
| D4 | 12.85 | | 2.54 | | 7.59 | | 44.61 | |
| D6 | 13.21 | | 4.48 | | 4.59 | | 41.27 | |
| D8 | 14.45 | | 3.60 | | 5.94 | | 39.38 | |
| V2 | 19.56 | 61.54 | 8.43 | 0.06 | 5.79 | 61.15 | 60.16 | 61.73 |
| V6 | 11.49 | 60.48 | 7.04 | 1.80 | 5.21 | 37.51 | 44.64 | 61.04 |
| V10 | 10.88 | 60.75 | 5.43 | 1.16 | 5.37 | 33.88 | 36.69 | 61.02 |
| V17 | 16.89 | 59.57 | 11.19 | 3.81 | 4.99 | 35.90 | 61.04 | 61.29 |
| V20 | 13.13 | 58.62 | 7.54 | 3.17 | 5.42 | 32.63 | 50.40 | 61.95 |
| V24 | 12.23 | 60.54 | 8.81 | 1.81 | 5.50 | 39.58 | 60.90 | 62.93 |
| V25 | 21.35 | 61.09 | 14.56 | 0.95 | 6.02 | 42.54 | 60.92 | 61.68 |

We can see that all time series show an average $A_{ACF}$ value of around 10 - 21 in the non-chatter regions. Those processes that show chatter have average $A_{ACF}$ values of 58.62 to 61.54 in the chatter regions. That is a large difference. One way to interpret the $A_{ACF}$ values is, as a measure of how much any measured value can be predicted by the preceeding 100 values. This however is not very close to the truth, because it does not account for shared predictive variance between different lag values. What Table ?? also shows it, that for all $V$-processes the variance of the $A_{ACF}$ values is lower in the *chatter* segments than in the *non-chatter* segments. This is not surprising, because

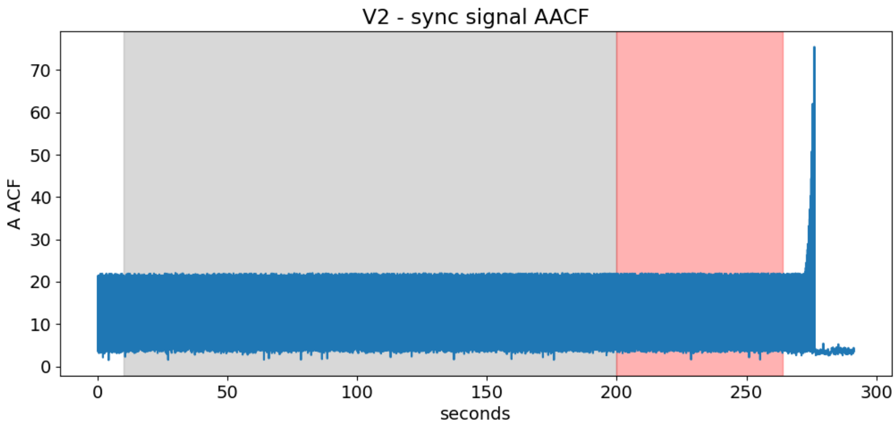


Figure 8: ACF for the *sync signal* variable of the *V2* process in two regions

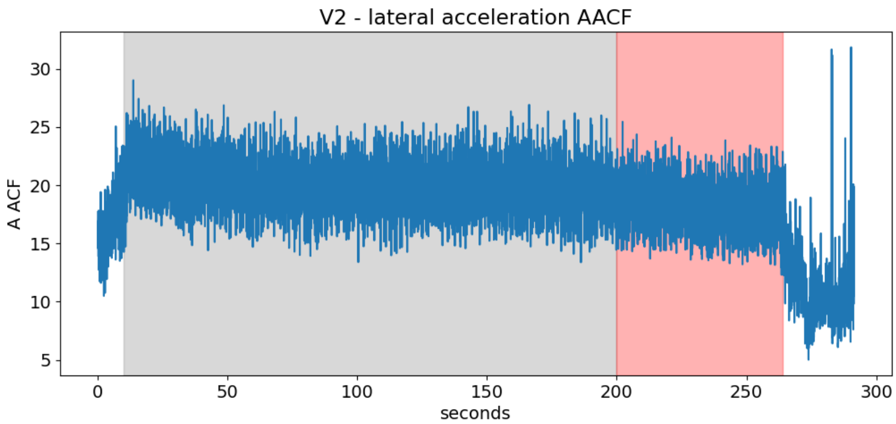


Figure 9: ACF for the *lateral acceleration* variable of the *V2* process in two regions

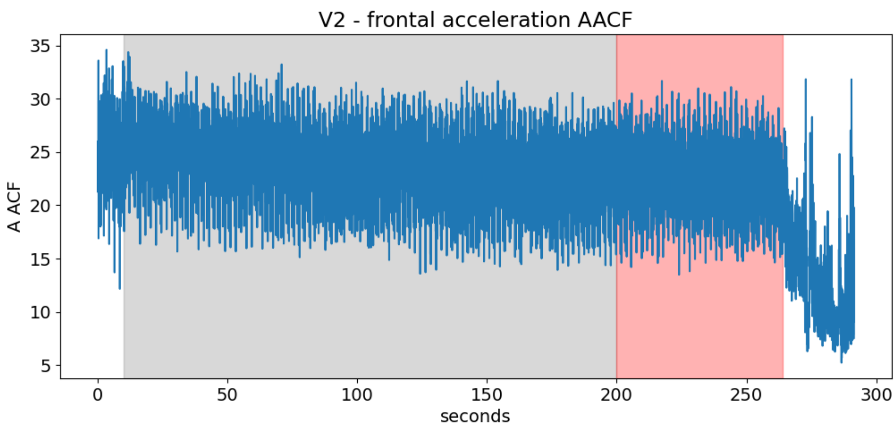


Figure 10: ACF for the *frontal acceleration* variable of the *V2* process in two regions

chatter is all about similar vibrations occuring for some time. But it is also true, that some chunks in the *non-chatter* segments have higher $A_{ACF}$ values that some chunks of the *chatter* region of the same process, as the *min* and *max* columns in the table show. So to develop a policy that allows us to detect chatter based on the $A_{ACF}$ value we need to take a closer look at some graphs.

Firstly plotting the $A_{ACF}$ value of the *moment* variable for each chunk of the $D$-processes shows us that the $A_{ACF}$ varies a bit but never reaches values greater than 45 (See Figure **??**, **??** and **??**).

For all of the $V$-processes we can see a similar behavior of the $A_{ACF}$ when entering the *chatter* region: The $A_{ACF}$ shoots up to a value around 60 and then stays relatively constant for almost the entire *chatter* period. During the *low chatter* segment, that often follows, the $A_{ACF}$ is a bit lower and not so low in variance, but still higher than when no chatter occurs. If we were to stop the machine as soon as the $A_{ACF}$ surpasses a value of 50, we are right in the beginning or the chatter in most cases. There is only one processe, *V25* where $A_{ACF}$ values occur during the normal boring process without being closely followed by chatter. This can be observed in Figure **??**. We now want to determine if the high $A_{ACF}$ values have predictive power that make a prediction leading up to the *chatter* region possible. It could also be that they only occur once we are already inside the chatter region, which would mean we would have to accept a little bit of chatter before the machine can be stopped. Going by the cutoff rule of $A_{ACF} = 50$ we can now determine for each $V$-process at which point in time the threshold is surpassed for the first time. Table **??** shows when the threshold of $A_{ACF} = 50$ is surpassed for the first time for each of the 7 $V$-processes. Negative values in the second column indicate that the threshold was reaches before being in the *chatter* segment.

Table 4: Time difference between the first point where $A_{ACF} > 50$ and start of *chatter* segment.

| process | time | difference |
|---|---|---|
| V2 | 199.85 s | -0.15 s |
| V6 | 47.15 s | 0.15 s |
| V10 | 47.15 s | 0.15 s |
| V17 | 34.15 s | -0.85 s |
| V20 | 51.45 s | -0.55 s |
| V24 | 21.55 s | -0.45 s |
| V25 | 23.25 s | -94.75 s |

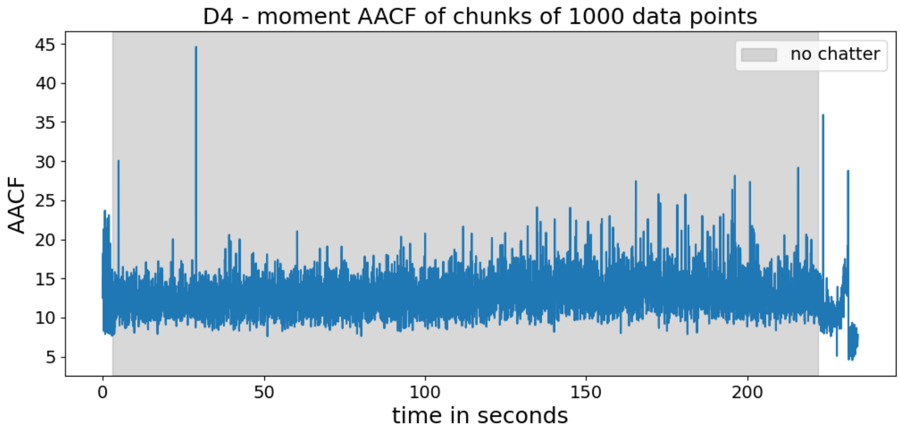


Figure 11: *D4* process: $A_{ACF}$ for *moment* variable

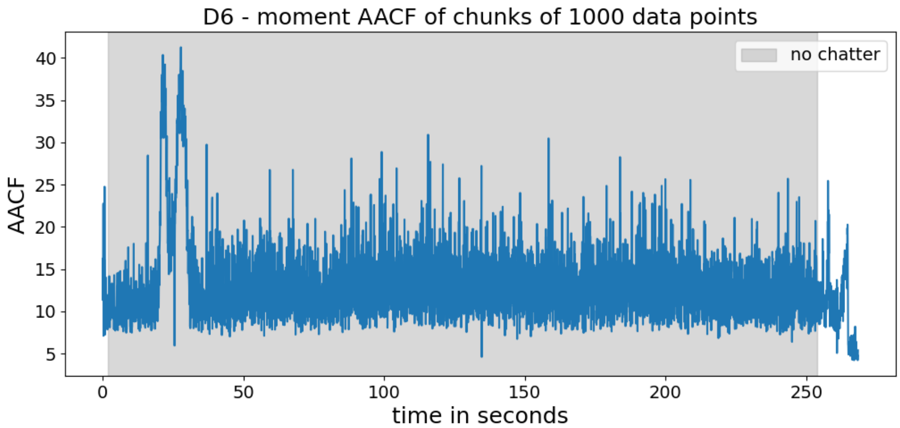


Figure 12: *D6* process: $A_{ACF}$ for *moment* variable

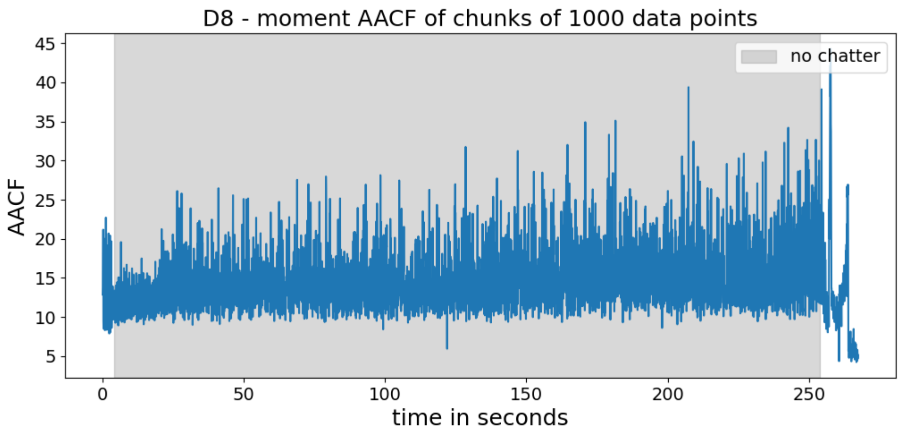


Figure 13: *D8* process: $A_{ACF}$ for *moment* variable

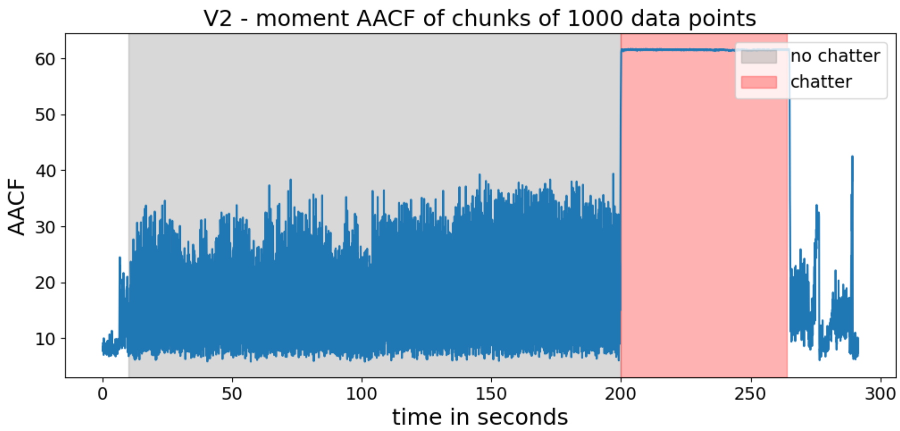


Figure 14: *V2* process: $A_{ACF}$ for *moment* variable

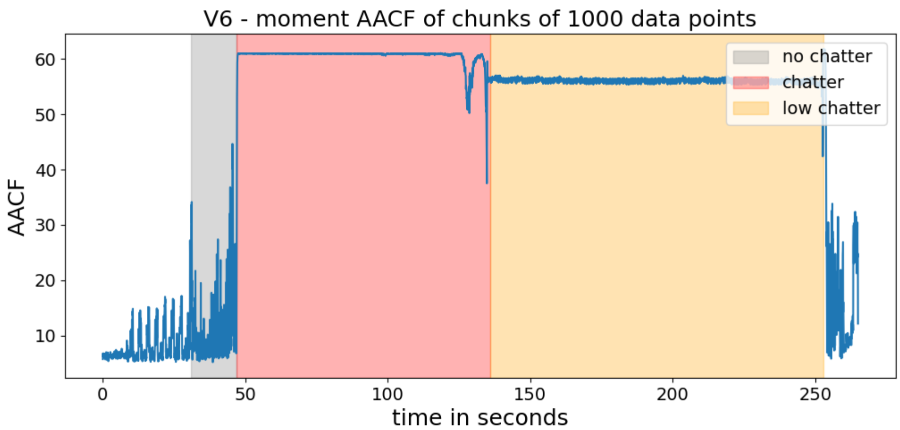


Figure 15: *V6* process: $A_{ACF}$ for *moment* variable

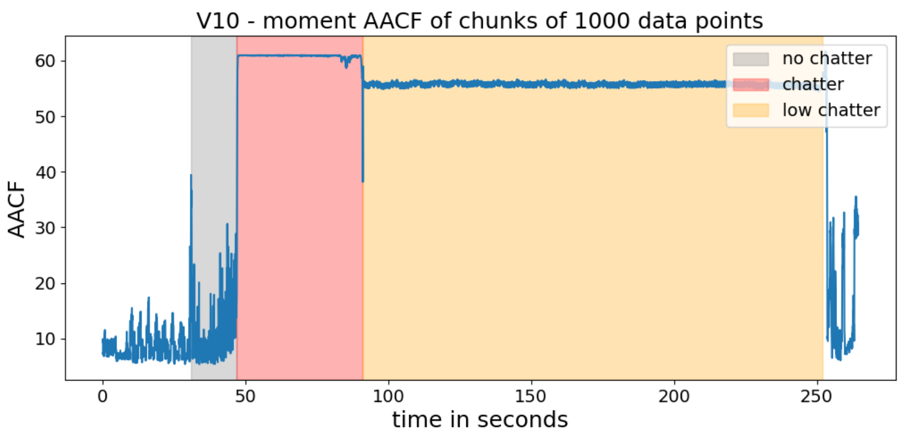


Figure 16: *V10* process: $A_{ACF}$ for *moment* variable

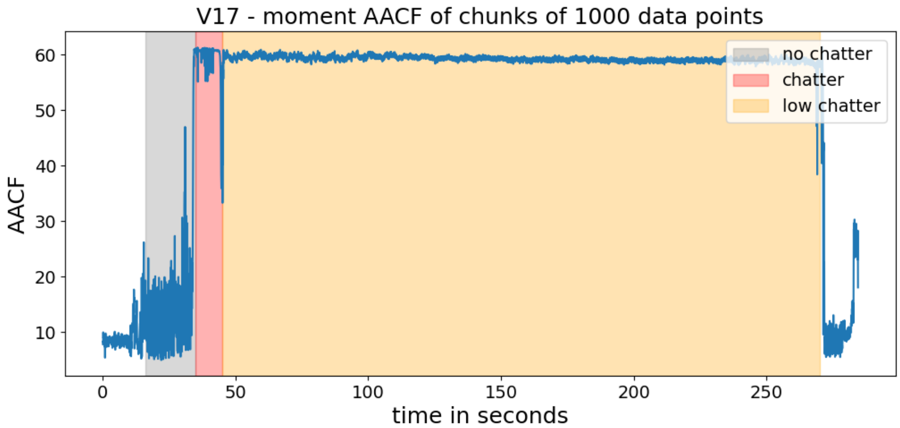


Figure 17: *V17* process: $A_{ACF}$ for *moment* variable

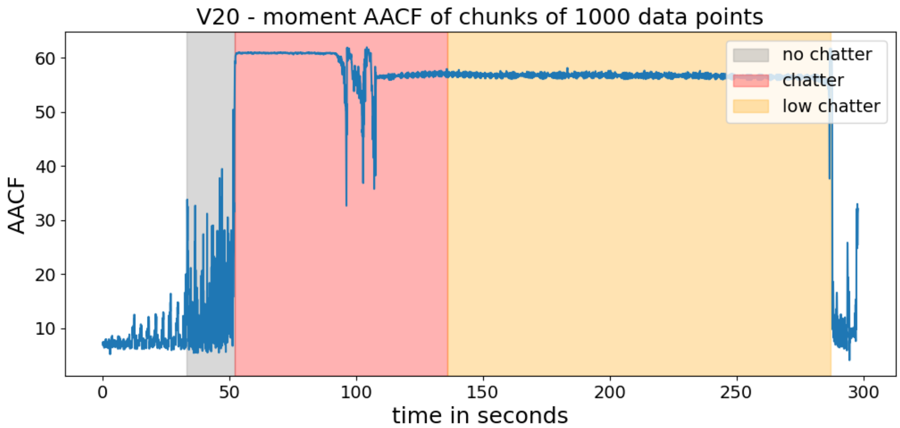


Figure 18: *V20* process: $A_{ACF}$ for *moment* variable

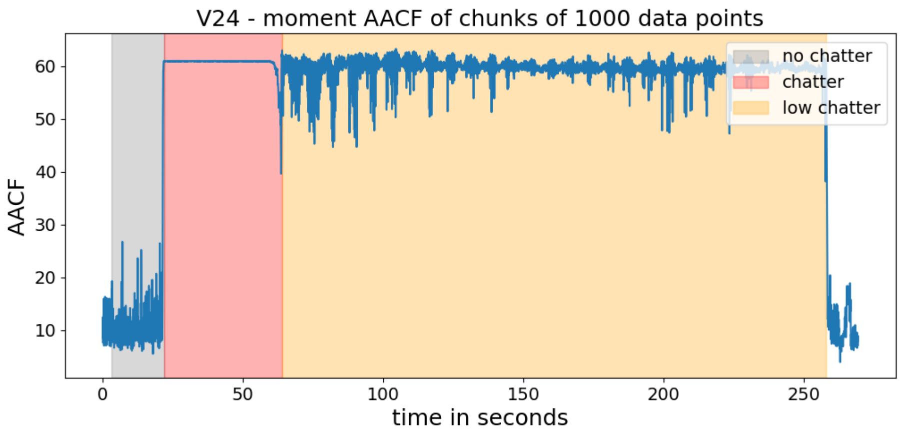


Figure 19: *V24* process: $A_{ACF}$ for *moment* variable

Out of the 7 processes, 6 were able to locate the start of chatter within a tolerance window of 1 seconds. Only process *V25* gave a very early alarm (See **??**). The *D*-processes which used a damper, never show $A_{ACF}$ values greater than 50, so the system does not seem to give false alarms if no chatter occurs at all. It is important to note that the exact value and sign of the difference should not be overinterpreted, as long as it is in the subsecond range. This is because the beginning and end time points of *chatter* and *non-chatter* regions were determined manually by listening to the audio signal. It is hard to tell the *exact* point in time when chatter starts. We do not want to investigate the *low chatter* regions that were determined by the same method. The objective of this report is, to find out how to predict the start of the chatter. Splitting chatter into *chatter* and *low chatter* was only done to have more uniform time segments to analyze. The *cutting speed*, *feed speed* and *oil pressure* parameters do not seem to differ much between the *D*-processes (no chatter) and *V*-processes we have data for.

# 4 Summary and Discussion

The quality and usefulness of our findings is hard to gauge because we determined the labels (*chatter* regions) on our own. Having hard labels for chatter and spiraling in the data would have been better for our analysis. We were able to show that out of all the variables, *moment* (drilling torque) showed the strongest difference between *chatter* and *non-chatter* regions. It is likely the best predictor variable for chatter as already found by **?** and (**?**, p. 27). In total, our analysis was not able to prove predictive power of the *moment* variable. The $A_{ACF}$ indicator was able to give good indications of the start of chatter in most cases. However it did not show any signs of chatter approaching in the seconds before the chatter was already there. Maybe it is enough though to stop the BTA machine as soon as the first signs of chatter appear. Using the drilling torque approach we presented, could however be a valuable alternative to listening to the acoustic signal manually in environments where there are a lot of acoustic disturbances. One point of contention in our approach could be the choice In addition to monitoring the *moment* variable, using a damper is probably the best measure that can be taken to avoid chatter all together. We are not sure about what disadvantages a damper could have for the drilling process. If we had more data, other approaches could be taken to predict chatte and stop the machine early. Having only 7 samples of drilling processes that show chatter in the data, is also not enough to perform statistical testing, as most statistical tests require at least 30 samples. A Recurrent neural network that is fed the different variables in the time or frequency domain might be able to learn patterns that predict chatter. But we do not have enough data to test this approach. It would also be interesting to see if the $A_{ACF}$ approach we chose in this report could also work for different work piece materials and BTA tool diameters.

# Bibliography


botek Präzisionsbohrtechnik GmbH. BTA - System. `https://www.botek.de/en/deep-hole-drilling/bta-system/`, 2023. URL `https://www.botek.de/en/deep-hole-drilling/bta-system/`.

Manfred Deistler and Wolfgang Scherrer. *Time Series Models*, volume 224. Springer Nature, 2022.

Michael Eid, Mario Gollwitzer, and Manfred Schmitt. *Statistik und Forschungsmethoden*. Beltz, 2017.

Charles R. Harris, K. Jarrod Millman, Stéfan J. van der Walt, Ralf Gommers, Pauli Virtanen, David Cournapeau, Eric Wieser, Julian Taylor, Sebastian Berg, Nathaniel J. Smith, Robert Kern, Matti Picus, Stephan Hoyer, Marten H. van Kerkwijk, Matthew Brett, Allan Haldane, Jaime Fernández del Río, Mark Wiebe, Pearu Peterson, Pierre Gérard-Marchant, Kevin Sheppard, Tyler Reddy, Warren Weckesser, Hameer Abbasi, Christoph Gohlke, and Travis E. Oliphant. Array programming with NumPy. *Nature*, 585(7825):357–362, September 2020. doi: 10.1038/s41586-020-2649-2. URL `https://doi.org/10.1038/s41586-020-2649-2`.

Tadeo Hepperle. gx1convert. `https://pypi.org/project/gx1convert/0.1.3/`, Year.

J. D. Hunter. Matplotlib: A 2d graphics environment. *Computing in Science & Engineering*, 9(3):90–95, 2007. doi: 10.1109/MCSE.2007.55.

pola-rs. polars: A python data manipulation library. `https://github.com/pola-rs/polars`, 2023.

Nils Raabe, Dirk Enk, Dirk Biermann, and Claus Weihs. Dynamic disturbances in bta deep-hole drilling: Modelling chatter and spiralling as regenerative effects. In *Advances in Data Analysis, Data Handling and Business Intelligence: Proceedings of the 32nd Annual Conference of the Gesellschaft für Klassifikation eV, Joint Conference with the British Classification Society (BCS) and the Dutch/Flemish Classification Society (VOC), Helmut-Schmidt-University, Hamburg, July 16-18, 2008*, pages 745–754. Springer, 2010.

Julius O. Smith. *Spectral Audio Signal Processing*. `http:`http://ccrma.stanford.edu/ jos/sasp//`/ccrma.stanford.edu/~jos/sasp/`, accessed <date>. online book, 2011 edition.

Winfried Theis. *Modelling varying amplitudes*. PhD thesis, Universität Dortmund, 2004.

Guido Van Rossum and Fred L. Drake. *Python 3 Reference Manual*. CreateSpace, Scotts Valley, CA, 2009. ISBN 1441412697.

Klaus Weinert, Oliver Webber, M Hüsken, and Jorn Mehnen. Statistics and time series analyses of bta deep hole drilling. In *International Conference on Non-linear Dynamics in Mechanical Processing*. Citeseer, 2001.

# Appendix

## A Additional figures

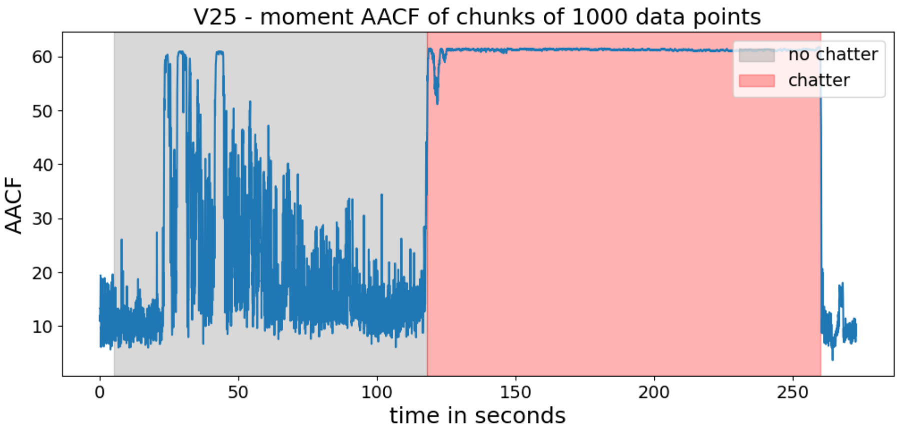


Figure 20: *V25* process: $A_{ACF}$ for *moment* variable

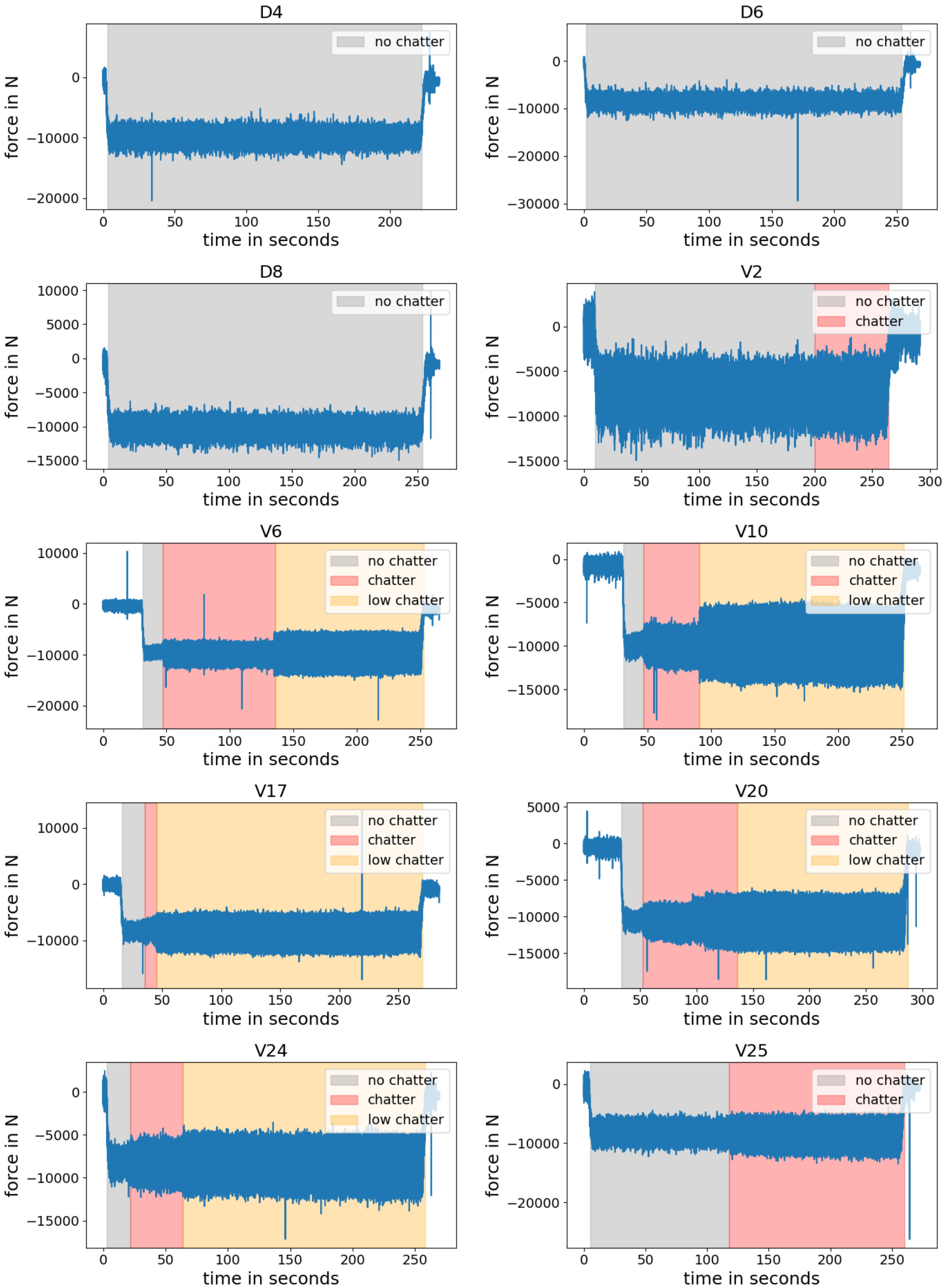


Figure 21: Force for all Processes

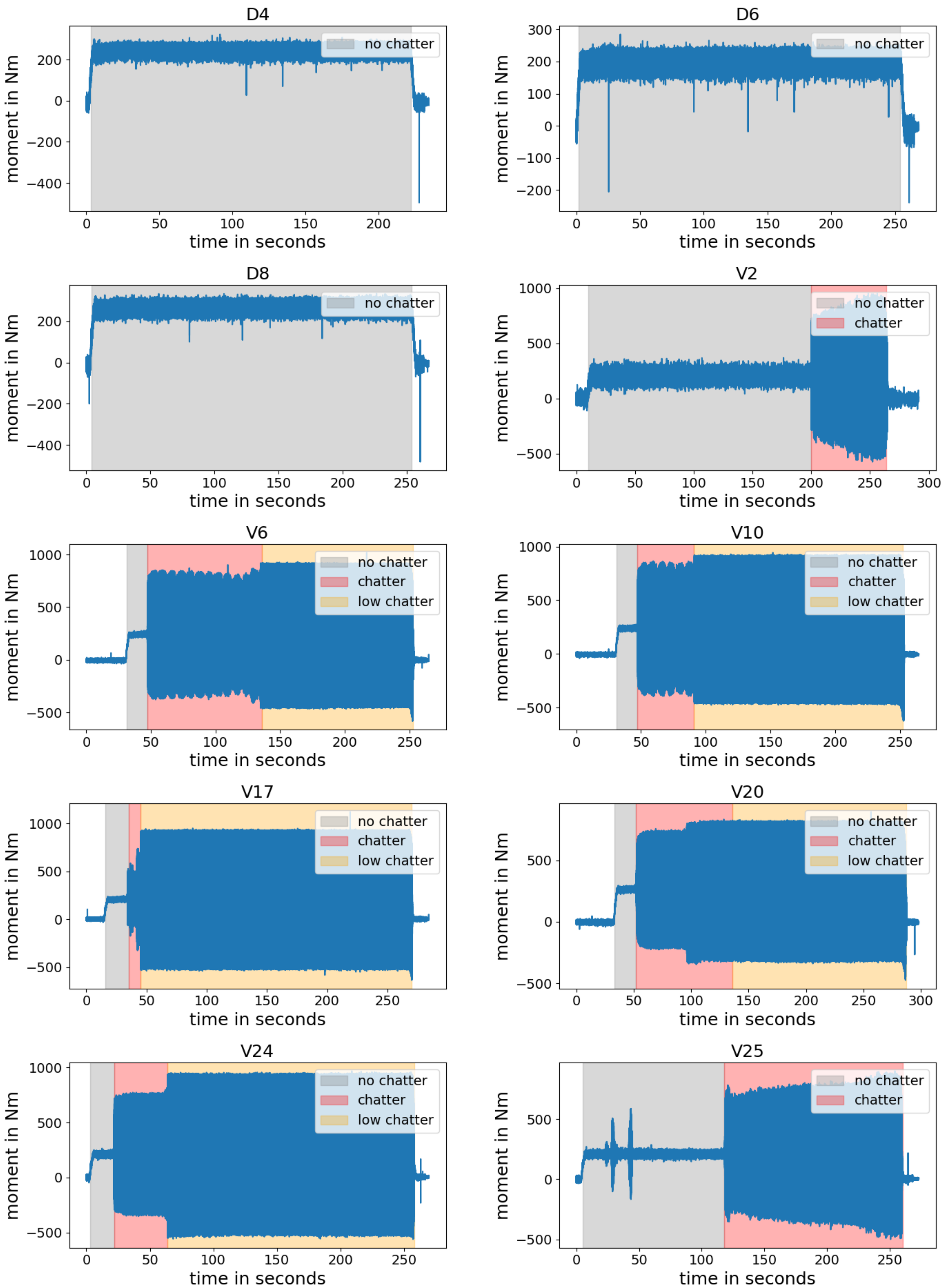


Figure 22: Moment for all Processes

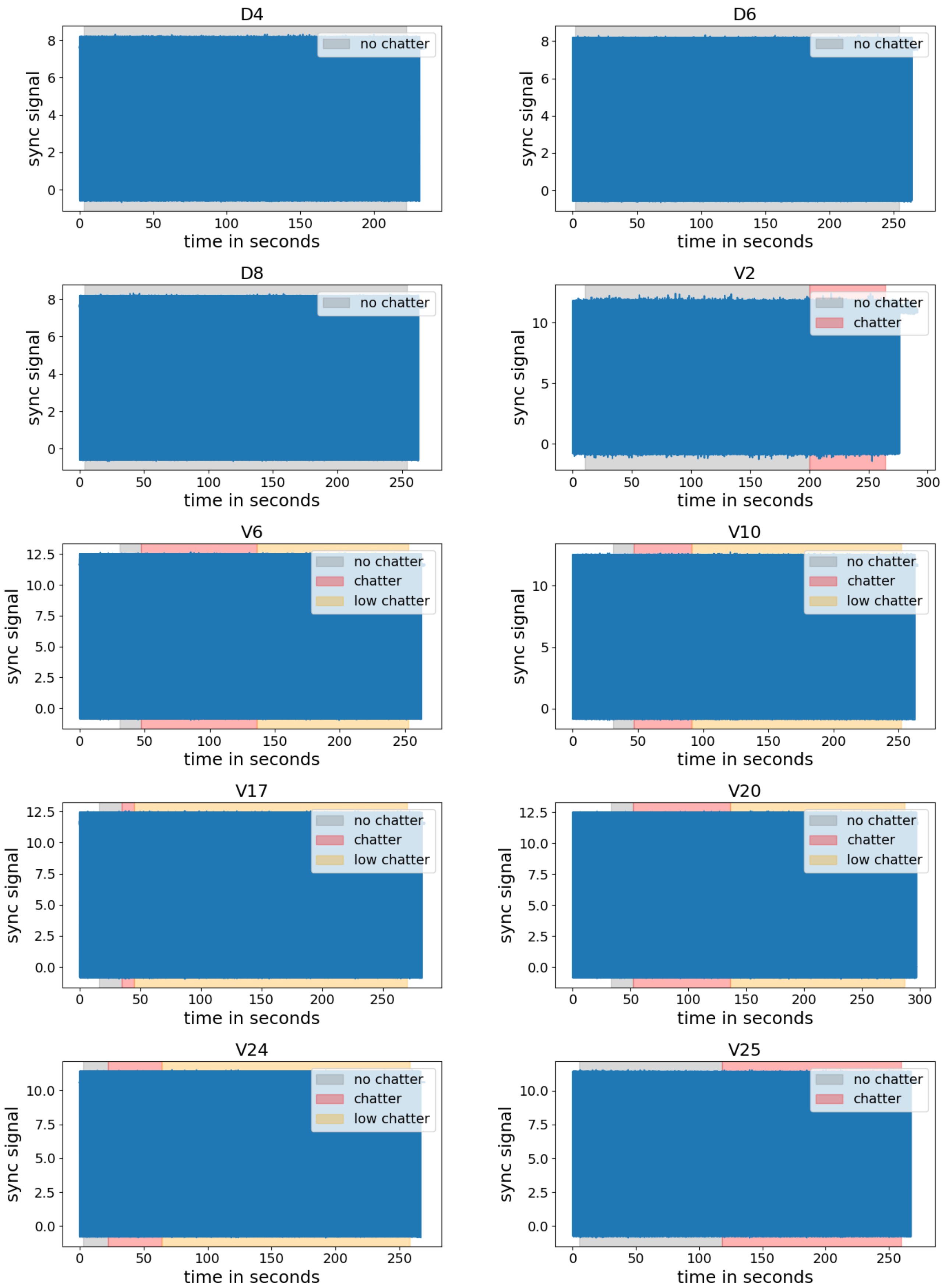


Figure 23: Sync Signal for all Processes

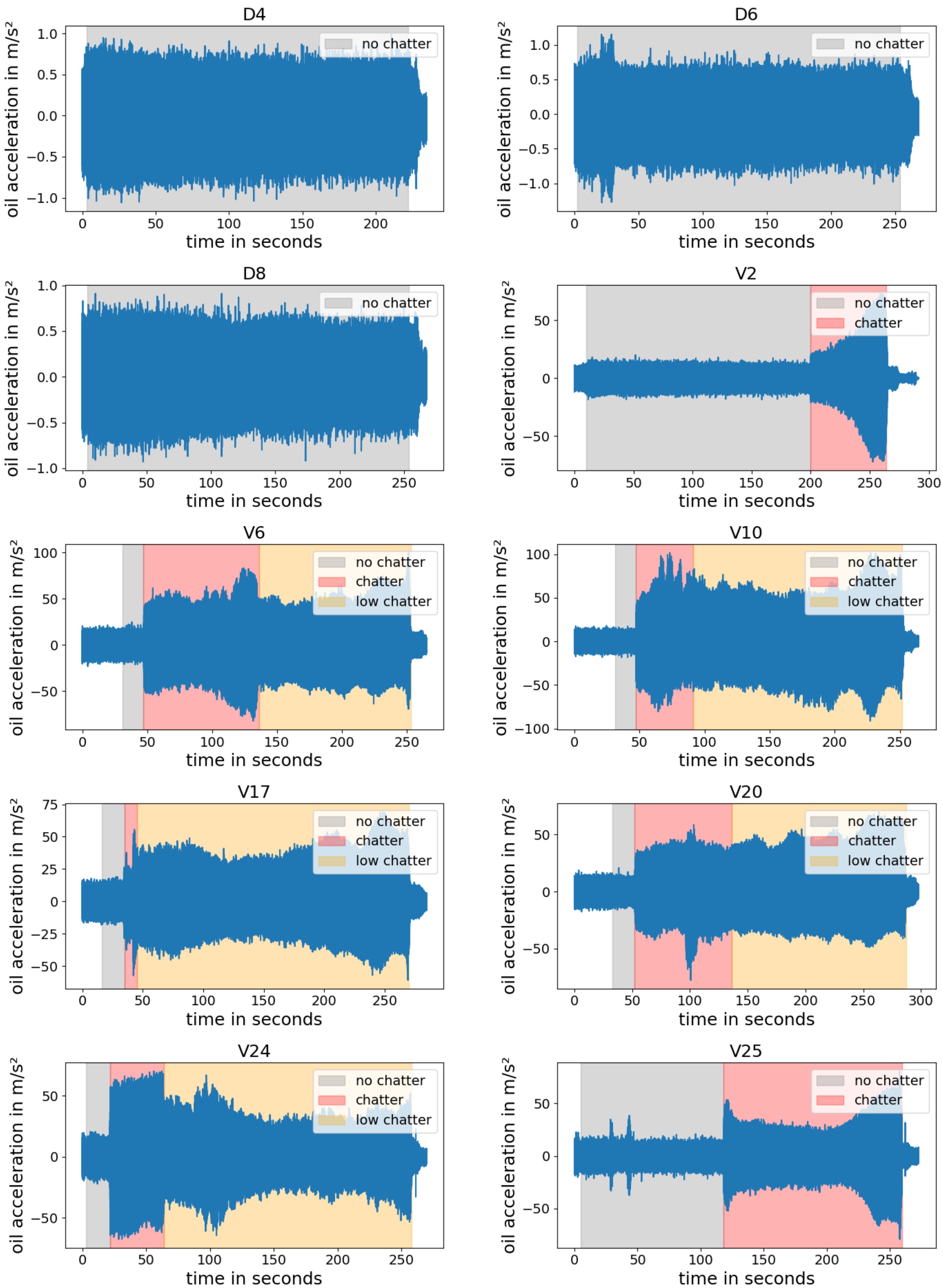


Figure 24: Oil Acceleration for all Processes

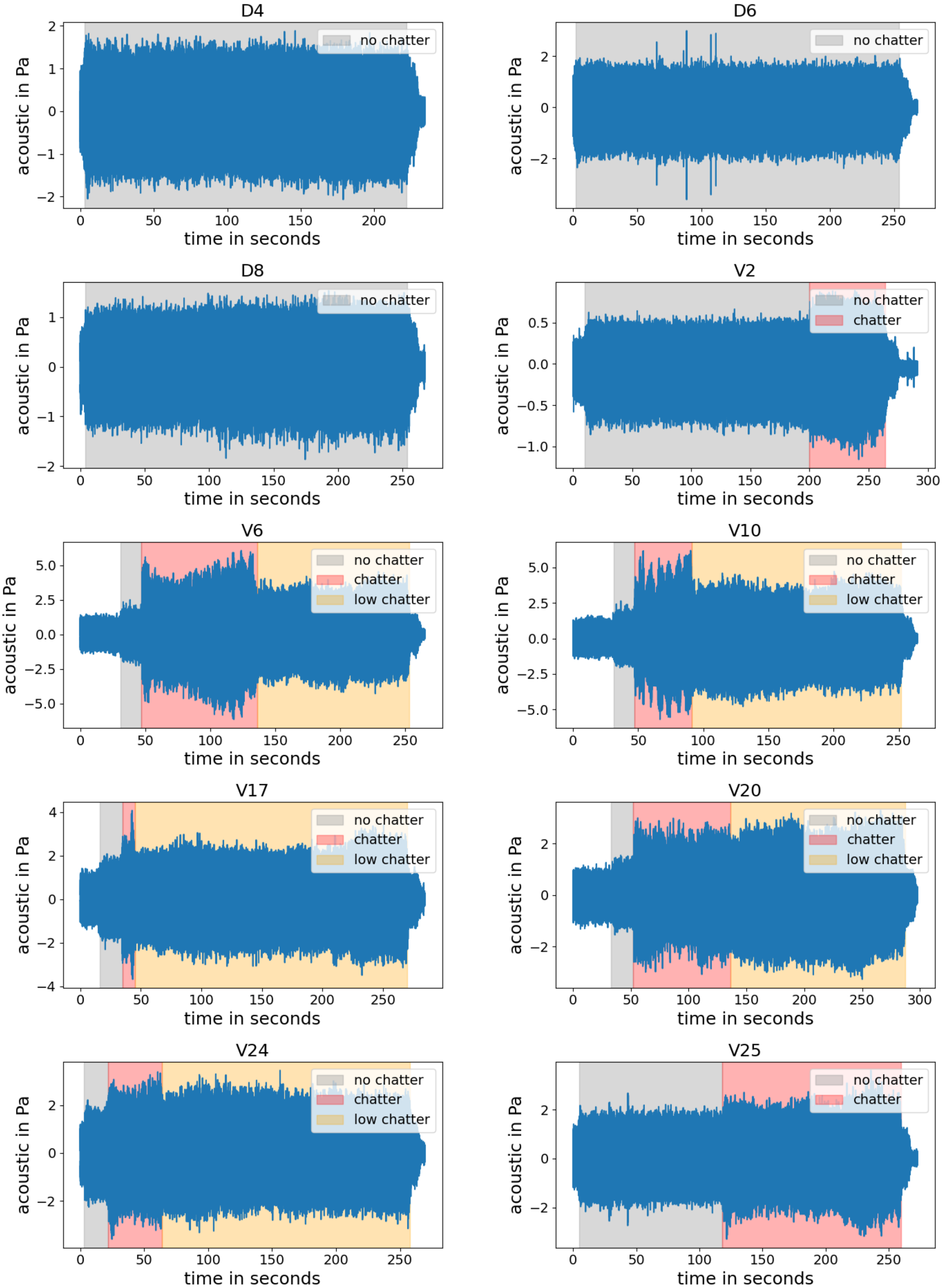


Figure 25: Acoustic for all Processes

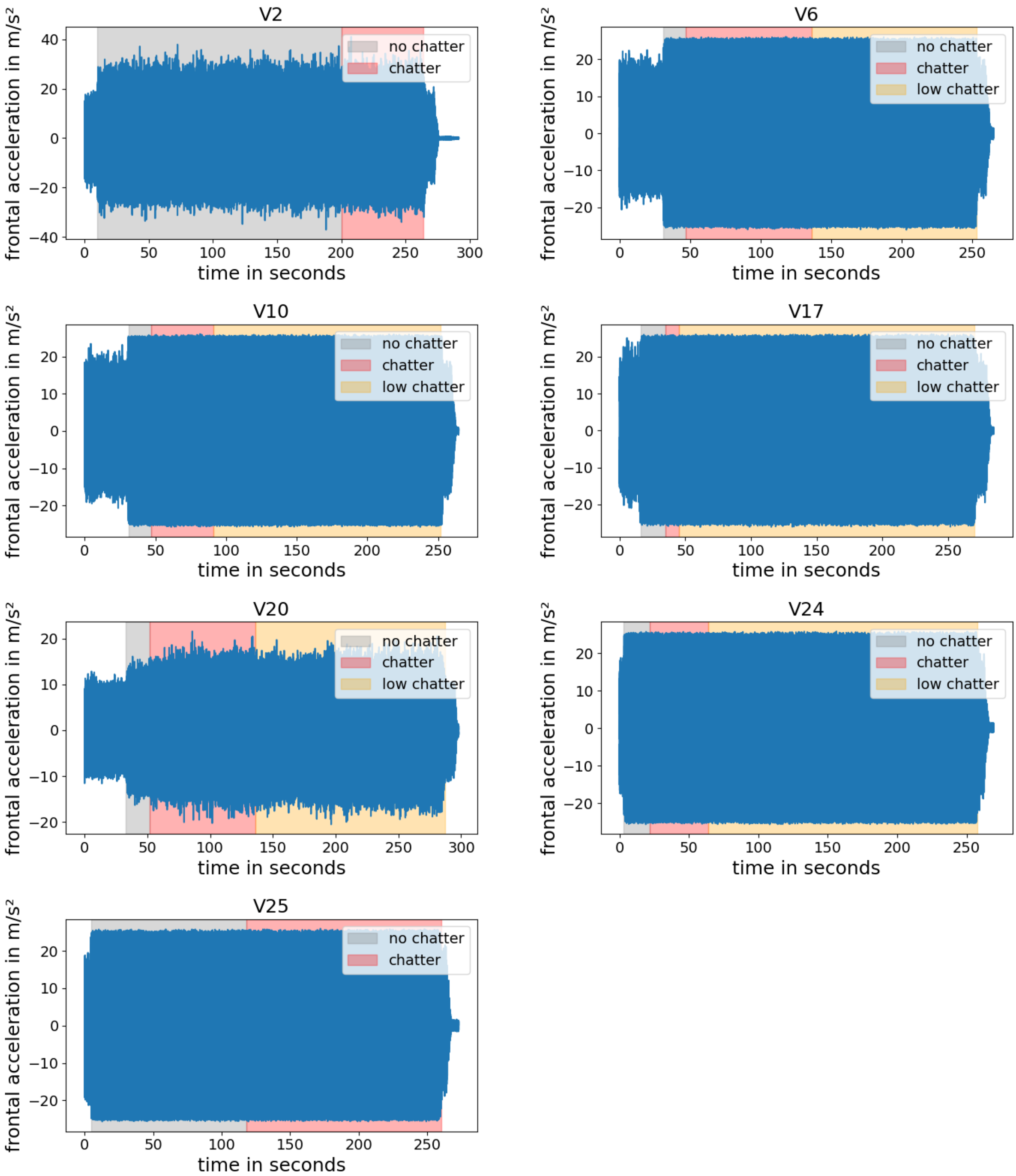


Figure 26: Frontal Acceleration for V-Processes

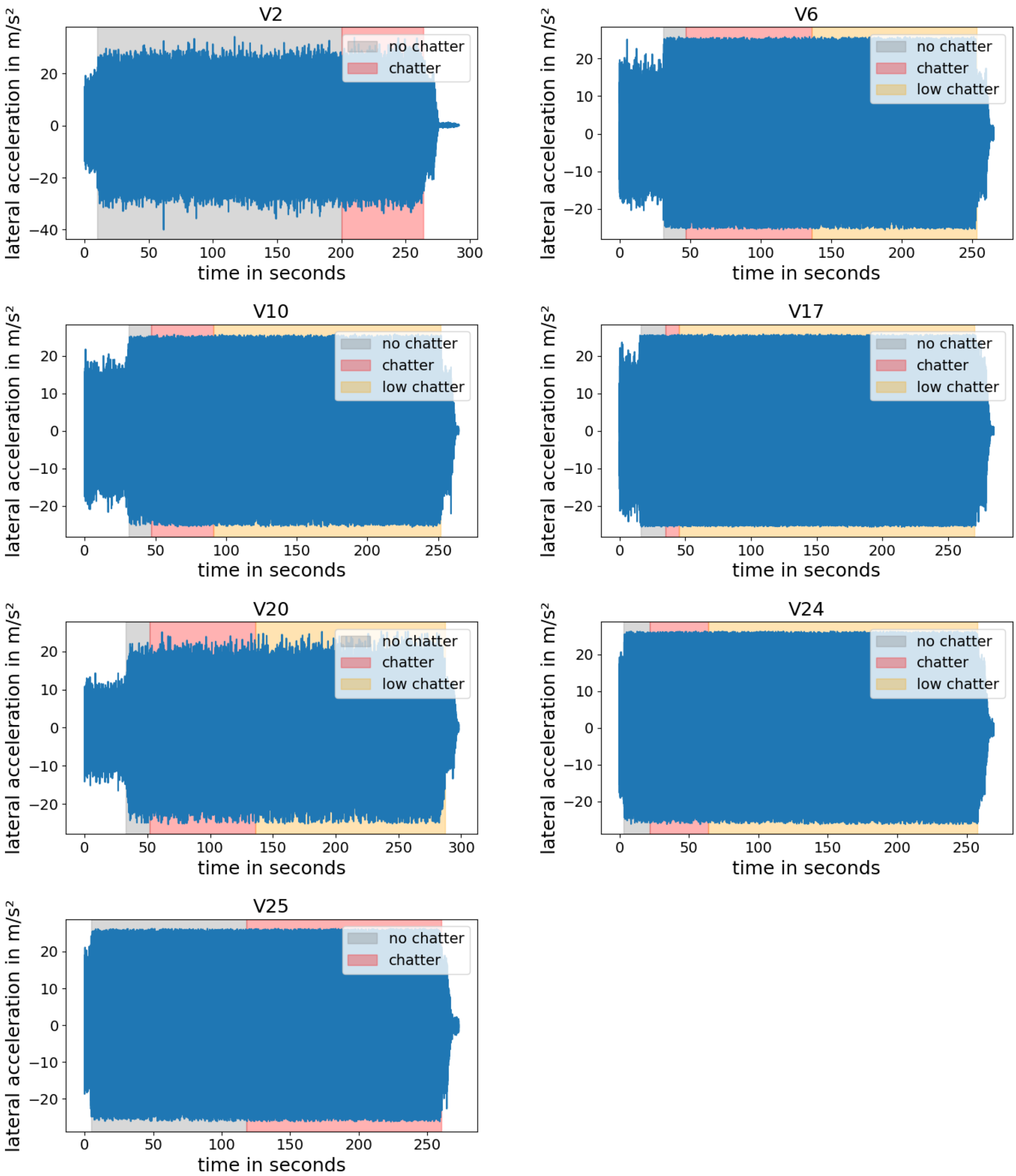


Figure 27: Lateral Acceleration for V-Processes